PCCP

Accepted Manuscript

This is an *Accepted Manuscript*, which has been through the Royal Society of Chemistry peer review process and has been accepted for publication.

Accepted Manuscripts are published online shortly after acceptance, before technical editing, formatting and proof reading. Using this free service, authors can make their results available to the community, in citable form, before we publish the edited article. We will replace this *Accepted Manuscript* with the edited and formatted *Advance Article* as soon as it is available.

You can find more information about *Accepted Manuscripts* in the **Information for Authors**.

Please note that technical editing may introduce minor changes to the text and/or graphics, which may alter content. The journal's standard **Terms & Conditions** and the **Ethical guidelines** still apply. In no event shall the Royal Society of Chemistry be held responsible for any errors or omissions in this *Accepted Manuscript* or any consequences arising from the use of any information it contains.

Rydberg dressing evolution via Rabi frequency control in thermal atomic vapors

Junling Che, Huaibin Zheng, Zhaoyang Zhang, Xin Yao, Cheng Li, Zhenkun Wu, Yanpeng Zhang[*]

Key Laboratory for Physical Electronics and Devices of the Ministry of Education & Shaanxi Key Lab of Information Photonic Technique, Xi'an Jiaotong University, Xi'an 710049, China

*Corresponding author: ypzhang@mail.xjtu.edu.cn

Abstract: We first report theoretical and experimental researches on Rydberg electromagnetically induced transparency and second-order fluorescence dressing evolution by Rabi frequency control in thermal atomic vapors, in which the controlled results are well explained by the dressing effect and Rydberg excitation blockade. Based on the certification of Rydberg excitation blockade fraction through the principle quantum number n dependence, we obtain the dressing evolution curves consisting of singly dressing and doubly dressing in local and nonlocal blockade sample by scanning probe and dressing fields. In addition, the competition between Rydberg dressing second-order fluorescence and fourth-order fluorescence is first investigated. The corresponding theory is given and consistent with experimental results. Such blockade evolution regularity has potential applications in the quantum control, and that Rydberg dressing can be useful in investigating many-body interactions as well as inducing short range interaction in Bose-Einstein condensate.

I. INTRODUCTION

Rydberg atoms with intriguing property[1] were investigated extensively in ultracold atoms in the last few years, which display strong interactions such as dipole-dipole interaction and van der Waals (vdW) interaction. The blockade effect[2,3] based on Rydberg atoms interaction can be used in quantum logic gates[4], which is a useful device for quantum computation[5] and quantum communication[6]. As one of the quantum coherent effects, electromagnetically induced transparency (EIT)[7,8] has been investigated intensively in the last two decades, which has much narrower width than natural line width and weak absorption so can contribute to study high-order nonlinear phenomenon[9-12]. In recently years, many investigations on Rydberg atoms in thermal environment also through EIT have been quite involved，which are more favorable than ultracold systems in terms of scalability and easy of use with respect to applications in quantum information. For example, nondestructive detection of the high excitation Rydberg states has been reported[13], GHz Rabi-Flopping involving Rydberg states have been observed[14], evidence for Rydberg van der Waals interaction has given[15]. However, these phenomena controlled by Rabi frequencies and blockade samples dressing interaction in thermal vapor has not been reported in experiment ever before.

In this paper, we study the EIT and multi-order fluorescence signals dressing evolution of

Rydberg states versus Rabi frequencies in a collective ensemble of rubidium thermal vapors in ladder-type three-level and Y-type four-level systems, where the interaction between the vdW blockade and singly- or doubly- dressing can be investigated. The dependences of the strengths of these signals are investigated to certify the existence of Rydberg excitation blockade fraction. With adding the external dressing field and scanning it, the competition of dressing effect between the Rydberg dressing second-order fluorescence and fourth-order fluorescence is investigated.

The article is organized as follows: in Sec. II, we exhibit the theoretical model and experimental scheme briefly; in Sec. III, we show the experimental results in detail, and meanwhile give the explanations according to the theoretical model. In Sec. IV, we conclude the article.

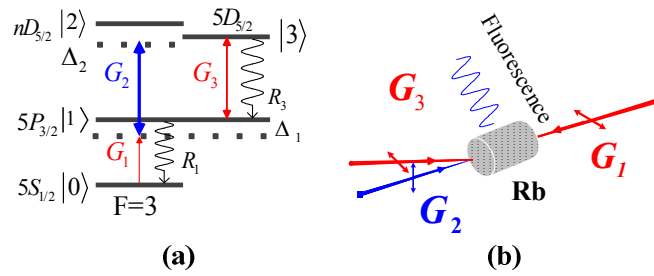## II. THEORETICAL MODEL AND EXPERIMENTAL SCHEME

(a)   (b)

Figure 1 (color online) (a) A Y-type four-level atomic system in ^{85}Rb atom for experimental processes, in which hyperfine state F=3 ($|0\rangle$) of the ground state $5S_{1/2}$, a first excited state $5P_{3/2}$ ($|1\rangle$), a low-lying excited state $5D_{5/2}$ ($|3\rangle$), and a highly-excited Rydberg state $nD_{5/2}$ ($|2\rangle$) are involved. (b) Simulate optical path of experiment. Double-headed arrows denote the polarizations of the incident beams, respectively.

A Y-type four-level atomic system shown in Fig. 1(a) is implemented in our experiment, which consists of the ground state $5S_{1/2}$, F=3 ($|0\rangle$), the first excited state $5P_{3/2}$ ($|1\rangle$), the second low-excited state $5D_{5/2}$ ($|3\rangle$) and a high-lying Rydberg state $nD_{5/2}$ ($|2\rangle$) of ^{85}Rb. The corresponding resonant frequencies are Ω_1, Ω_2, Ω_3 for transitions $|0\rangle\rightarrow|1\rangle$, $|1\rangle\rightarrow|2\rangle$ and $|1\rangle\rightarrow|3\rangle$, respectively. Three external cavity diode lasers (ECDLs) are used to couple the corresponding transition Rabi frequencies. The Rabi frequency is $G_i=\mu_i E_i/\hbar$ (i=1, 2, 3), where $\mu_i \propto K=|\langle J||er||J'\rangle|=\sqrt{3\varepsilon_0 h\lambda^3(2J'+1)\big/[16\pi^3\tau(2J+1)]}$ is the electric dipole moment, $\tau\propto n^3$ is the lifetime. So $G_i\propto n^{-3/2}$ can be obtained through analyzing the above relation. A weak beam $\mathbf{E}_1$ (wave vector $\mathbf{k}_1$, frequency ω_1, Rabi frequency G_1) probes the transition $|0\rangle\rightarrow|1\rangle$ with the wavelength of 780.24 nm. Two couple beams $\mathbf{E}_2$ ($\mathbf{k}_2$, ω_2, G_2) and $\mathbf{E}_3$ ($\mathbf{k}_3$, ω_3, G_3) drive the transition $|1\rangle\rightarrow|2\rangle$ with the wavelength ~480 nm and $|1\rangle\rightarrow|4\rangle$ with the wavelength 775.98 nm, respectively. All these light beams are spatially designed as shown in Fig. 1(b), in which $\mathbf{E}_2$ and $\mathbf{E}_3$ transmit through the rubidium vapor cell in the same direction with the small angle (~0.3°), $\mathbf{E}_1$ propagates in the opposite direction of $\mathbf{E}_2$.

Considering the level $|2\rangle$ being the Rydberg state, an approximate mean-field model is used to

2

depict as following: Because of the strong interaction of Rydberg atoms, a spherical domain is defined. In this domain, only one atom is excited to $|2\rangle$ and the other at low states. The entire sample is divided into many domains, which have the same radius R_b, defined as the blockade radius. So, R_b will determine the number of Rydberg atoms in the sample and the distance between two Rydberg atoms. The Rydberg state $|2\rangle$ in a domain is shifted by other nearby Rydberg atoms outside the domain. The local density ρ_0 of atoms at ground state is assumed uniform in the domain. According to the condition of single Rydberg atom within a domain, we have $\rho_e V_d=1$, in which V_d is the spherical volume, and the density ρ_e of Rydberg atoms is defined uniform inside and around the spherical domain, which is given by

$$\rho_e = C\rho_0^{0.2}\,|\,G_1\,|^{0.4}\left(|\,G_2\,|\,/\,n^{11}\right)^{0.4}. \tag{1}$$

Therefore, the condition $\rho_e V_d=1$ can be transformed into $\rho\int_{V_d}d^3r|c_2(r,t)|^2 = 1$, in which the integral variable r is the radial coordinate from the domain origin and $c_2(r, t)$ the r-dependent probability amplitude of atoms exited to $|2\rangle$. Considering that the strong van der Waals interaction of Rydberg atoms for nD state is $V_{DD} = -C_5/R^5 - C_6/R^6 - C_7/R^7$ [16], so the energy shift ε of an atom in one domain can be described as

$$\varepsilon(r,t) = \rho_e\int_{V'}d^3r'(-C_5/|r'-r|^5 - C_6/|r'-r|^6 - C_7/|r'-r|^7), \tag{2}$$

where $r'{\geq}R_d$ and V' runs over the entire volume outside the domain. Now, we substitute the energy shift ε into the nonlinear Bloch-like equations as

$$i\dot{c}_1(r,t) = G_2 c_2(r,t)/2,$$

$$i\dot{c}_2(r,t) = -\varepsilon c_2(r,t) + G_2 c_1(r,t)/2, \tag{3}$$

in which $c_1(r, t)$ is the r-dependent probability amplitude of atoms excited to state $|1\rangle$. Based on Eq. (3), we can obtain the numerical relationship between $\varepsilon(r)$ and r. So the average energy shift should be $\Delta E = \int_0^{R_d}\varepsilon(r)dr$. After this treatment, a strict calculation of energy level shift can be obtained.

Two energy-level systems comprised of ladder-type three-level and Y-type four-level subsystems will be investigated with and without $\mathbf{E}_3$. There is only one EIT window $|0\rangle{\leftrightarrow}|1\rangle{\leftrightarrow}|2\rangle$ if $\mathbf{E}_3$ is absent, and will be two EIT windows $|0\rangle{\leftrightarrow}|1\rangle{\leftrightarrow}|2\rangle$ and $|0\rangle{\leftrightarrow}|1\rangle{\leftrightarrow}|3\rangle$ if $\mathbf{E}_3$ is considered. Generally, the expressions of the density-matrix elements, the imaginary part of $\rho_{10}^{(1)}$ related to the probe transmission process proportionally determines the strength of the probe transmission signal, $\rho_{11}^{(2)}$, $\rho_{22}^{(4)}$ and $\rho_{33}^{(4)}$ related to the different second-order and fourth-order fluorescence processes proportionally determine the fluorescence signal intensity, can be obtained by solving the coupled density-matrix equations[17].

For probe transmission signals, the corresponding first-order density matrix $\rho_{10}^{(1)}$ is

$$\rho_{10}^{(1)} = i\,|\,G_1\,|\,/d_1 \tag{4}$$

Considering the singly dressing and the blockade effect of $\mathbf{E}_2$ in mean field model, the expression of $\rho_{10}^{(1)}$ can be modified as

$$\rho_{10D}^{(1)} = i\,|\,G_1\,|^{0.2}\,/[d_1 + (|\,G_2\,|\,/n^{11})^{0.4}\,/d_2]\,, \tag{5}$$

Next, considering the doubly dressing of $\mathbf{E}_2$ and $\mathbf{E}_3$, the expression of $\rho_{10}^{(1)}$ can be given by

$$\rho_{10DD}^{(1)} = i\,|\,G_1\,|^{0.2}\,/[d_1 + (|\,G_2\,|\,/n^{11})^{0.4}\,/d_2 + |G_3|^2\,/d_3]\,, \tag{6}$$

where $d_1 = \Gamma_{10} + i\Delta_1$, $d_2 = \Gamma_{20} + i(\Delta_1 + \Delta'_2)$, $\Delta'_2 = \Delta_2 + \varepsilon$, $d_3 = \Gamma_{30} + i(\Delta_1 + \Delta_3)$. Frequency detuning is defined as $\Delta_i = \Omega_i - \omega_i$.

On the order of above methods to achieve second-order fluorescence signal R_1 (excited by beam $\mathbf{E}_1$ and radiated from level $|1\rangle$), the density-matrix element $\rho_{11}^{(2)}$ via perturbation chain $\rho_{00}^{(0)} \xrightarrow{E_1} \rho_{10}^{(1)} \xrightarrow{(E_1)^*} \rho_{11}^{(2)}$ is

$$\rho_{11}^{(2)} = -\,|\,G_1\,|^2\,/(d_1\Gamma_{11})\,. \tag{7}$$

Considering the dressing of $\mathbf{E}_2$ and blockade effect, the expression of $\rho_{11}^{(2)}$ can be modified as

$$\rho_{11D1}^{(2)} = -\,|\,G_1\,|^{0.4}\,/[\Gamma_{11}(d_1 + G_2^{0.4}\,/n^{4.4}d_2)]\,. \tag{8}$$

By introducing the dressing of $\mathbf{E}_3$ when scanning Δ_2, the equation will be modified to

$$\rho_{11DD1}^{(2)} = -\,|\,G_1\,|^{0.4}\,/[\Gamma_{11}(d_1 + G_2^{0.4}\,/n^{4.4}d_2 + |\,G_3\,|^2\,/d_3)]\,. \tag{9}$$

The corresponding doubly dressing Rydberg second-order fluorescence intensity I_{D1} can be described as

$$I_{D1} = \rho_0 \times \rho_{11DD1}^{(2)}\,. \tag{10}$$

Then considering the dressing of $\mathbf{E}_3$ and $\mathbf{E}_2$ when scanning Δ_3, $\rho_{11}^{(2)}$ is substituted by

$$\rho_{11D2}^{(2)} = -\,|\,G_1\,|^{0.4}\,/[\Gamma_{11}(d_1 + |\,G_3\,|^2\,/d_3)]$$

$$\rho_{11DD2}^{(2)} = -\,|\,G_1\,|^2\,/[\Gamma_{11}(d_1 + G_2^{0.4}\,/n^{4.4}d_2 + |\,G_3\,|^2\,/d_3)] \tag{11}$$

The corresponding doubly dressing second-order fluorescence intensity I_{D2} can be described as

$$I_{D2} = \rho_0 \times \rho_{11DD2}^{(2)} \tag{12}$$

The Rydberg fourth-order fluorescence R_2 (excited by $\mathbf{E}_1 \& \mathbf{E}_2$ and radiated from level $|2\rangle$) is described by $\rho_{00}^{(0)} \xrightarrow{E_1} \rho_{10}^{(1)} \xrightarrow{E_2} \rho_{20}^{(2)} \xrightarrow{(E_1)^*} \rho_{21}^{(3)} \xrightarrow{(E2)^*} \rho_{22}^{(4)}$. Taking the dressing of $\mathbf{E}_3$ into account, the expression of density-matrix element $\rho_{22}^{(4)}$ and its intensity I_2 can be obtained.

$$\rho_{22}^{(4)} = \frac{G_1^{0.4} G_2^{0.4}}{n^{4.4}\Gamma_{22}d_2\{d_1 + \frac{|G_1|^2}{\Gamma_{11}} + \frac{|G_3|^2}{d_3} + \frac{|G_2|^{0.4}}{n^{4.4}d_2}\}[\Gamma_{21} + i\Delta_2 + \frac{|G_1|^2}{d_2} + \frac{|G_3|^2}{\Gamma_{23} + i(\Delta_2 - \Delta_3)} + \frac{|G_2|^{0.4}}{n^{4.4}\Gamma_{22}}\}}$$

$$I_2 = \rho_0 \times \rho_{22}^{(4)}. \tag{13}$$

The density-matrix element $\rho_{33}^{(4)}$ and intensity I_3 for non-Rydberg fourth-order fluorescence R_3 (excited by $\mathbf{E}_1 \& \mathbf{E}_3$ and radiated from level $|3\rangle$) can be obtained in a similar way as

$$\rho_{33}^{(4)} = \frac{G_1^2 G_3^2}{\Gamma_{33}d_3[d_1 + \frac{G_2^{0.4}}{n^{4.4}d_2} + \frac{|G_3|^2}{d_3}][\Gamma_{31} + i\Delta_3 + \frac{G_2^{0.4}}{n^{4.4}[\Gamma_{32} + i(\Delta_3 - \Delta_2)]} + \frac{|G_3|^2}{\Gamma_{33}}]}$$

$$I_3 = \rho_0 \times \rho_{33}^{(4)}. \tag{14}$$

without the dressing effect, by $\rho_{00}^{(0)} \xrightarrow{E_1} \rho_{10}^{(1)} \xrightarrow{E_3} \rho_{30}^{(2)} \xrightarrow{(E_1)^*} \rho_{31}^{(3)} \xrightarrow{(E_3)^*} \rho_{33}^{(4)}$.
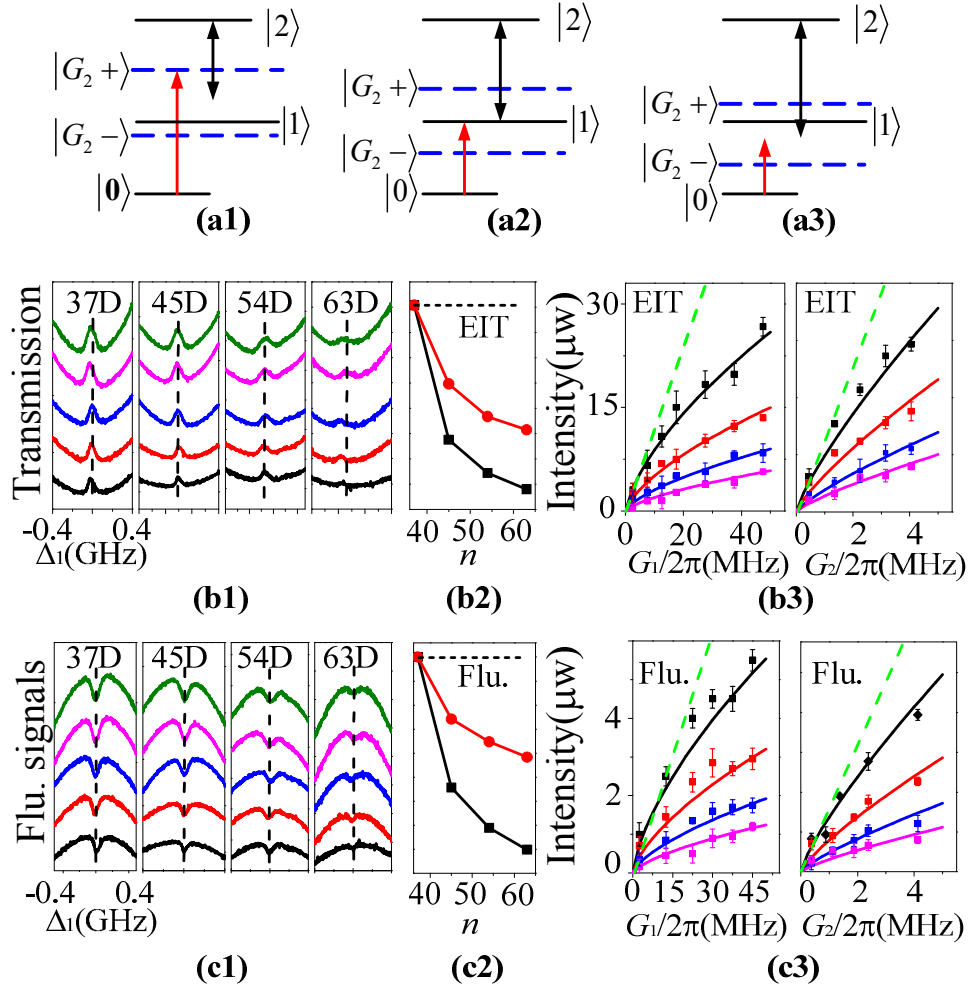
III. RESULTS AND DISCUSSIONS

Figure 2 (color online). (a) Dressing energy level diagrams if $\Delta_2 > 0$ (a1), $\Delta_2 = 0$ (a2) and $\Delta_2 < 0$ (a3). (b1) The EIT spectrums of different n (37D, 45D, 54D, and 63D, respectively) are measured versus Δ_1 at various

Rabi-frequencies. (b2) Dependence of EIT intensity on n. (b3) Dependences of EIT intensity on G_1 and G_2. (c) Figure setup is as (a), but for second-order fluorescence signals. The error bars in (b3) and (c3) represent the standard deviation of repeated measurements. The atoms density is 1×10^{12} cm^{-3}.

By blocking E_3 and scanning probe field, the singly dressing evolution curves by Rabi frequency control in Rydberg local blockade sample are presented. Rydberg EIT window within the Doppler absorption dip is generated in the ladder-type three-level subsystem ($|0\rangle \leftrightarrow |1\rangle \leftrightarrow |2\rangle$), which means EIT satisfying the two-photon resonance condition $\Delta_1 + \Delta_2 = 0$ of the term $|G_2|^{0.4}/[\Gamma_{20} + i(\Delta_1 + \Delta_2)]$ in Eq. (5). It is well known that the probe transmission can be controlled by dressing effect of light field. But Rydberg blockade can shift the energy level so that compete with dressing effects. The dressing effect of $\mathbf{E}_2$ split level $|1\rangle$ into two primary dressed states $|G_2 \pm\rangle$ as displayed by the singly dressing energy level diagrams in Fig. 2(a). When $\Delta_2 = 0$, the strongest EIT peak appears at $\Delta_1 + \Delta_2 = 0$ and represents the strongest dressing effect. When $\Delta_2 < 0$, $\Delta_1 > 0$ scan from small to large around $|G_2+\rangle$ so that generate the weaker Rydberg EIT spectra and dressing effect in experiment. Similarly, When $\Delta_2 > 0$, $\Delta_1 < 0$ scan from small to large around $|G_2-\rangle$ so that also observe the weaker Rydberg EIT spectra.

By fixing $\Delta_2 = 0$, Fig. 2(b1) shows the experimental EIT spectrums at different G_1 (from top to bottom) corresponding to four different Rydberg states (from left to right) 37D, 45D, 54D and 63D, respectively. When different n is considered at the same $G_1(G_2)$ value, the principle quantum n dependence is shown in Fig. 2(b2), where the dashed line is defined as the pure signal; the square curve is the height of the measured EIT spectrum. In order to directly study the relationship between the blockade strength and principle quantum number n, we must avoid the dipole transition probability μ_{ij} which can lead to the decrease of EIT and fluorescence strengths with n increasing. Because accounting for the probe transmission is determined by Im[$\rho_{10}^{(1)}$], the measured EIT spectrum is determined by Im[$\rho_{10D}^{(1)}$]-Im[$\rho_{10}^{(1)}$]. Thus the experimental EIT spectrum intensity can be expressed as $I_{\text{EIT}} = \text{Im}\{iG_1|G_2|^2/d_2(d_1 + |G_2|^2/d_2)\}$. Because G_2 is weak, we can get $I_{\text{EIT}} \propto |G_2|^2$. It is well known that $G_2 \propto \mu_{ij} \propto n^{-3/2}$ so $I_{\text{EIT}} \propto n^{-3}$. As a result we scale the measured values to $n=37$ by a factor $(n/37)^3$ to obtain the dot curve in Fig. 2(b2), which can directly certify that the Rydberg blockade fraction exists, and become stronger with n increasing. This phenomenon can be understood with Eq. (5). The term of $(|G_2|/n^{11})^{0.4}/d_2$ of $\rho_{10D}^{(1)}$ proportionally determined the intensity of EIT peak created by $\mathbf{E}_2$. With n increasing, the $(|G_2|/n^{11})^{0.4}/d_2$ becomes smaller, so the Rydberg EIT spectrum becomes weaker.

After certifying the existence of the Rydberg blockade fraction, we can observe the interplay between the singly dressing and local blockade with different Rabi frequencies. Figure 2(b3) presents Rydberg EIT spectrum for different states (37D, 45D, 54D and 63D) as function of Rabi-frequency G_1 and G_2, respectively. The intensity values are also scaled by the factor $(n/37)^3$ to avoid the dipole transition μ_{ij} influence. In order to depict visually, the standard intensity I_{crit} without blockade and

dressing effect is plotted in Fig. 2(b3). The EIT spectrum intensity for four high n numbers, which are obtained via Lorenz fitting, coincides with I_{crit}. When G_1 (G_2) is small, because the Rydberg atoms are sparse sufficiently that the Rydberg level shift $\varepsilon = 0$. As G_1 (G_2) increasing, the effect of blockade and dressing on EIT spectra both appear gradually and influence each other, which make the EIT spectra deviate from the standard intensity. Then the distance between the intensity value of different n and I_{crit} become larger because the effect of dressing and blockade gets strong. Anatomizing principle quantum number n from 37 to 63 in Fig. 2(b3) under each definite Rabi-frequency, we find that the blockade effect becomes strong but the dressing effect does not change. So these evolution curves clearly show the interaction between the dressing effect and increasing gradually blockade effect. This regularity can also be understood with Eq. (5), where $\rho_{10D}^{(1)}$ is direct proportion to $G_1^{0.2}$ and $(|G_2|/n^{11})^{0.4}/d_2$. When G_1 and G_2 increase the value variation of $G_1^{0.2}$ and $G_2^{0.4}$ make the blockade effect and dressing effect of $\mathbf{E}_2$ become stronger and the growth rate of this EIT becomes slow. The solid lines in Fig. 2(b3) are theoretical simulations which agree with the experimental results.

In order to reveal these competitions more clearly, a series of Rydberg dressing second-order fluorescence signals in the EIT window are shown in Fig. 2(c) corresponding to Fig. 2(b). In general, the second-order fluorescence emitted from $|1\rangle$ is modulated by $\mathbf{E}_2$. The Rydberg dressing second-order fluorescence dip generates due to the dressing of $|2\rangle$, which can be determined by density matrix $\rho_{11D1}^{(2)}$ (Eq. (8)). The Rydberg fourth-order fluorescence represented by $\rho_{22}^{(4)}$ is emerged by double photon resonance, which can be observed in low atomic states in our experiment. By analyzing Eq. (13), we can estimate that the Rydberg fourth-order fluorescence $\rho_{22}^{(4)}$ become smaller with the increasing of n mainly due to $\rho_{22}^{(4)} \propto 1/n^{4.4}$, as a result the fourth-order fluorescence signals $\rho_{22}^{(4)}$ of Rydberg states cannot be observed in our experiments. The same scaling method is used because I_{D1} can be depicted as $I_{D1} \propto |G_1|^2|G_2|^2/\Gamma_{11}^2 d_1 d_2$. Therefore, $I_{D1} \propto n^{-3}$ can be obtained. We can derive the Rydberg second-order fluorescence substantial regularity as function of Rabi-frequency G_1(G_2) in Fig. 2(c3). On the basis of analysis above, each Rydberg dressing second-order fluorescence dip can be determined by the term $G_1^{0.4} G_2^{0.4}/d_1 d_2$ in $\rho_{11D1}^{(2)}$, which can directly reflect the blockade interact with dressing effect. With the Rabi-frequency G_1(G_2) increasing, a dramatical suppression appears which makes the dip be shallower, and such suppression becomes stronger with n increasing. The physical interpretation of this result is that the system in a superposition where blockaded Rydberg atoms can not be excited and thereby contribute to the Rydberg dressing second-fluorescence signals have the relation of $\rho_{11D1}^{(2)} \propto G_1^{0.4}$ and $\rho_{11D1}^{(2)} \propto G_2^{0.4}$ in theory, so the Rydberg dressing second-fluorescence $\rho_{11D1}^{(2)}$ cannot be enhanced linearly any longer.

Next, we utilize another better experimental way scanning dressing field[18] which can make the Doppler absorption dip (in probe channel) and Doppler emission peak (in fluorescence channel) as free background and directly observe the dressing effect to further investigate singly dressing evolution in the strong Rydberg blockade sample with ladder-type three-level subsystem $|0\rangle \leftrightarrow |1\rangle \leftrightarrow |2\rangle$. With the couple laser being scanned around $|2\rangle$, the experimental signals of different n about G_1 are shown in Figs. 3(a1) and (a2). Figure 3(b) shows the Rydberg probe transmission variation directly at Δ_1 discretely by scanning dressing field Δ_2 in detail. In the probe transmission signals, the heights of baselines (horizontal background) represent Doppler absorption background which is due to the term d_1 in $\rho_{10D}^{(1)}$ at corresponding Δ_1, as shown by the dashed curves in Fig. 3(b). In every curve in Fig. 3(b), a peak appears with Δ_2 scanned, which the EIT spectrum is created by Rydberg state $|2\rangle$. So the condition of $\Delta_1+\Delta_2+\varepsilon=0$ is satisfied in every peak due to the relation of $|G_2|^{0.4}/[\Gamma_{20}+i(\Delta_1+\Delta_2+\varepsilon)]$. The height of EIT peak becomes stronger when $|\Delta_1|$ changes from big to small. In order to understand the phenomenon, we similarly resort to the singly dressing energy diagrams shown in Fig. 3(c). When $|\Delta_1|=0$ (α) and Δ_2 is scanned, the EIT spectrum and corresponding singly dressing effect are strongest due to the suppressing condition $\Delta_1+\Delta'_2=0$ is satisfied and the probe field $\mathbf{E}_1$ is not resonant with either of the two dressed energy levels $|G_2\pm\rangle$, as shown in Fig. 3(c3). In the region $\Delta_1<0$ ($\Delta_1>0$), the probe field is resonant with $|G_2+\rangle$ ($|G_2-\rangle$), thus the enhancement condition $\Delta_1 + (\Delta'^2_2 + \sqrt{\Delta'^2_2 + 4G_2^2})/2 = 0$ $(\Delta_1 + (\Delta'^2_2 - \sqrt{\Delta'^2_2 + 4G_2^2})/2 = 0)$ is satisfied and the EIT spectrum as well as the corresponding singly dressing are the weakest.

In the region with Δ_1 changing from -0.4 GHz to 0 and from 0 to 0.4 GHz, the singly dressing depicted by the term $G_2^{0.4}/n^{4.4}d_2$ become strong with Δ_1 approaching to 0. So the Rydberg EIT spectrum becomes weaker. The case with $|\Delta_1|=0$ (α) is same as Fig. 2 but the consistence of experimental data and theory prediction by scanning dressing field is better than the case by scanning the probe field. We find that the accuracy of scanning probe field (Fig.2) is 15%~20% and scanning dressing field (Fig.3) is 5%~10%. Especially, when $|\Delta_1|=0.4$ GHz (β), interaction of Rydberg atoms is the strongest due to weak nonlinear absorption in this nonlocal blockade[19], which can help us to distinctly study the interaction with Rabi frequency under the condition of weak singly-dressing and strong blockade effect. But the weakest dressing make the Rydberg EIT spectrum can not been observed by scanning probe field so that we must choose scanning dressing field.

Now, by scanning dressing field, we obtain the principle quantum number n dependence in Figure 3(d), which reflects the variation of the Rydberg blockade. Akin to the scaling method mentioned above, we obtain the red dot curve; the vertical distance between the curve and dashed line represents the Rydberg blockade fraction strength, with the principle number n increasing, the EIT strengths in Fig. 3(d) weaken, which can be explained by changing the blockade term ρ_e in Eq. (1). With n

increasing, $\rho_e = C\rho_0^{0.2}|G_1|^{0.4}(|G_2|/n^{11})^{0.4}$ gets smaller, so EIT intensity weakens. Figure 3(e1) is the evolution about G_1 and G_2, which is consistent with Fig. 2(b3) but the distance between different n are bigger and the evolution can increase to saturation with G_1 increasing, which can illustrate that blockade effect is stronger than dressing effect in this condition. So blockade effect makes the evolution curves saturation and the bigger n is, the smaller Rabi frequency is required to saturation. Rydberg dressing evolution can be simulated by Eq. (5), as shown by the solid lines in Fig. 3(e1), which can display the regularity more clearly.
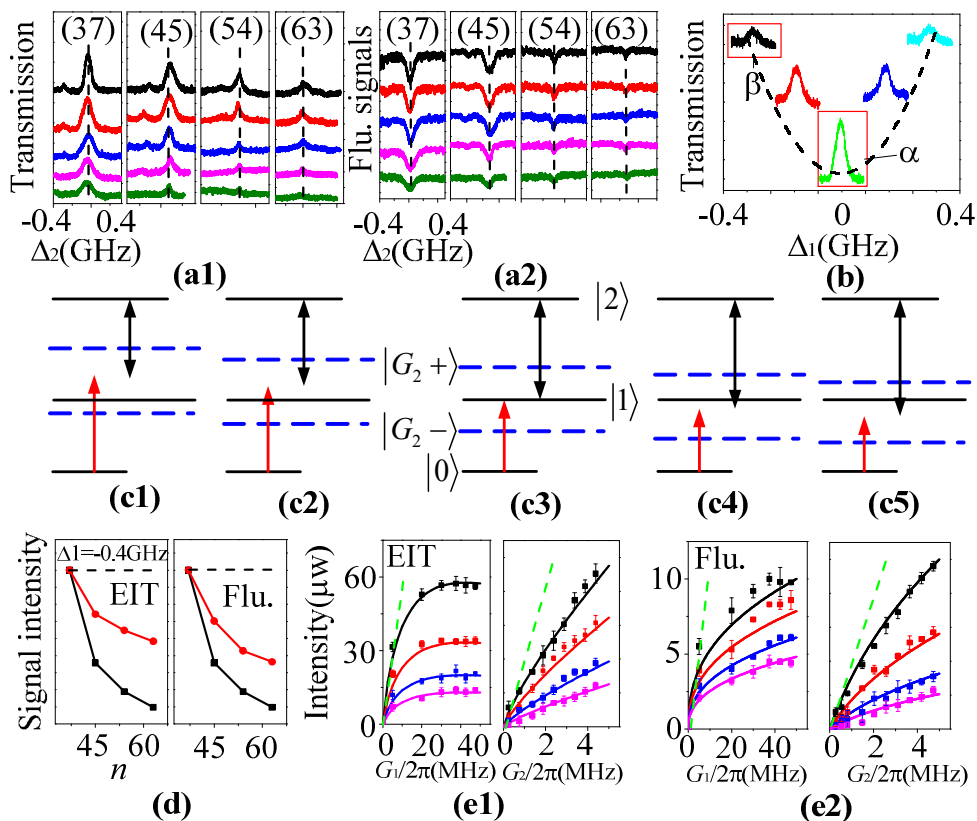

Figure 3 (color online). EIT, second-order fluorescence signals and Rabi frequency dependence curves versus Δ_2. (a1) Measured spectrums of EIT when the Δ_1 at the location of α. (a2) Setup is as (a1) but for second-order fluorescence signals. (b) Different detune Δ_1 versus Δ_2. α is $\Delta_1=0$, β is $\Delta_1=-50$MHz. (c) Dressed energy level diagrams when (c1) $\Delta_1=-0.3$GHz, (c2) $\Delta_1=-0.1$GHz, (c3) $\Delta_1=0$, (c4) $\Delta_1=0.1$GHz, (c5)$\Delta_1=0.3$GHz. (d) Principle quantum number n dependences are related to EIT and second-order fluorescence intensity, respectively, when $\Delta_1=-0.3$GHz. (e) Intensity dependence curves of EIT spectrums (e1) and second-order fluorescence signals (e2) with different G_1 and G_2, respectively, when $\Delta_1=-0.3$GHz. The error bars in (e1) and (e2) represent the standard deviation of repeated measurements. Dots represent the original experimental data and the solid curves are the theoretic simulation.

To further reveal the weak singly dressing interact with strong blockade, we show the Rydberg second-order fluorescence signals in Fig. 3(a2) corresponding to the probe transmission signals in Fig.

3(a1). Meanwhile, n (Fig. 3(d)) and G_1&G_2 (Fig. 3 (e2)) dependence curves are shown. It is obvious that regularity of second-order fluorescence signals $\rho_{11D1}^{(2)}$ is similar with the Fig. 2. However, each dependence curve in Fig. 3(e) bends more greatly. This result can further represent the strong blockade effect distinctly influence dressing effect. With n increasing, the value of $G_2^{0.4}/n^{4.4}d_2$ become small, the strong blockade effect make the second-order fluorescence signals $\rho_{11D1}^{(2)}$ get weaker. With G_1 (G_2) increasing, the blockade effect is more significant, which can result in that the signal intensities increase from linear to nonlinear even saturation. In addition, theoretical simulation curves on the basis of $\rho_{11D1}^{(2)} \propto G_1^{0.4}G_2^{0.4}$ in Fig. 3(e2) are consistent with the experiment.
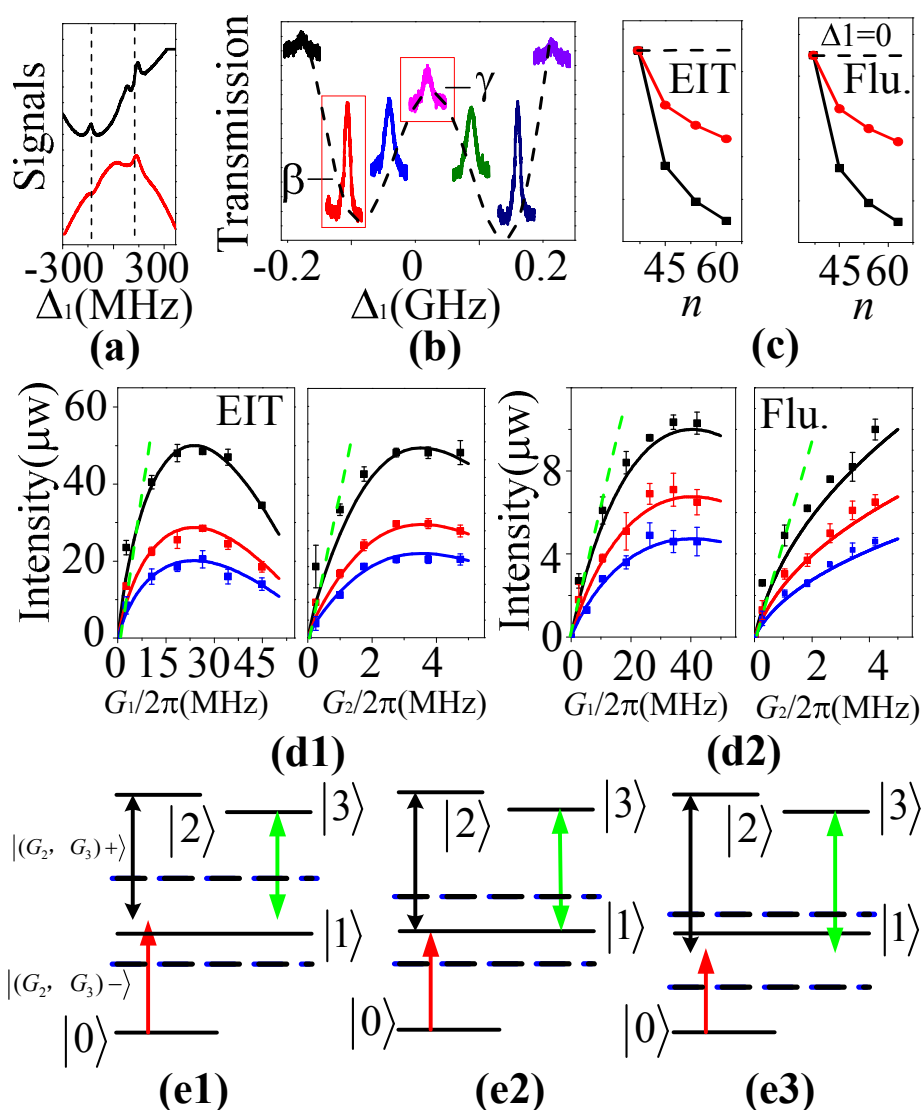

Figure 4 (color online) (a) Double EIT (upper curve) and coexisting second-order and fourth-order fluorescence signals (lower curve) versus Δ_1. (b) EIT signals versus Δ_2 at different Δ_1. (c) Intensity of EIT and second-order fluorescence signals for different n versus Δ_2 with Δ_1=0. (d) Dependence curves of (d1) the evolution of EIT

intensity and (d2) Second-order fluorescence signal for 37D, 45D and 54D when $\Delta_1=0$ on $G_1\&G_2$. (e) Doubly-dressed energy-level diagrams: (e1) $\Delta_1<0$, (e2) $\Delta_1=0$, (e3) $\Delta_1>0$. The error bars in (d1) and (d2) represent the standard deviation of repeated measurements. Dots represent the original experimental data and the solid curves are the theoretic simulation.

To study the interaction between Rydberg blockade and doubly dressing, we add an external dressing field $\mathbf{E}_3$ to investigate in Y-type four-level subsystem. In this case, there are two ladder subsystems $|0\rangle\leftrightarrow|1\rangle\leftrightarrow|2\rangle$ and $|0\rangle\leftrightarrow|1\rangle\leftrightarrow|3\rangle$ interplaying with each other, doubly dressing dark state can be generated. Two ways can be adopted to obtain the experimental results, by scanning Δ_1 and Δ_2, respectively. Figure 4(a) presents the measured EIT and second-order fluorescence signals by scanning Δ_1. The right EIT peak at $\Delta_3=300$ MHz in the top curve is caused by $\mathbf{E}_3$ and the left one at $\Delta_2=-300$ MHz by $\mathbf{E}_2$. The corresponding second-order fluorescence spectrum is shown in the lower curve. A fourth-order fluorescence peak $\rho_{33}^{(4)}$ emitted from $|3\rangle$ is located inside its dressing second-order fluorescence dip $\rho_{11D2}^{(2)}$ caused by $\mathbf{E}_3$. However, because of $\mathbf{E}_2$, only a Rydberg dressing second-order fluorescence dip $\rho_{11D1}^{(2)}$ appears.

Now, by scanning Δ_2 in discrete Δ_1 we study the interaction between the Rydberg blockade and doubly dressing. Fig. 4(b) shows the EIT spectrum via scanning the frequency detuning Δ_2 and Δ_1 discretely changed among the curves in every panel. On the basis of doubly-dressed energy level diagram in Fig. 4(e), the doubly dressing makes $|1\rangle$ totally split into four dressed state. Firstly, under the external-dressing of $\mathbf{E}_3$, $|1\rangle$ can be dressed into primarily dressed state $|G_3\pm\rangle$. Simultaneously, $|1\rangle$ can be decomposed into primarily dressed state $|G_2\pm\rangle$ due to self-dressing of $\mathbf{E}_2$. We assume the symcenters of $|G_2\pm\rangle$ and $|G_3\pm\rangle$ overlap to interpret our experimental results, the eigenvalues of dressed state $\lambda_1=\sqrt{|G_1|^2+|G_3|^2}$, $\lambda_2=0$ and $\lambda_3=\sqrt{|G_1|^2+|G_3|^2}$ can be obtained through solving secular equation. Then, in the region $\Delta_1<0$, when Δ_2 is scanned around $|(G_2, G_3)+\rangle$, the signals satisfy the enhancement condition $\Delta_1+\Delta_2'+\sqrt{|G_2|^2+|G_3|^2}=0$. So, the EIT spectrums are lower than the signals which are resonant with Δ_1. Symmetrically, in the region $\Delta_1>0$, scanning Δ_2 around $|(G_2, G_3)-\rangle$, the signals satisfied $\Delta_1+\Delta_2'-\sqrt{|G_2|^2+|G_3|^2}=0$ are small. When $\Delta_1=0=-\Delta_2-\varepsilon=-\Delta_3$, the signals satisfy the suppression condition $\Delta_1+\Delta_2+\varepsilon=0$, so the corresponding dressing is the strongest and the EIT peak reaches the highest point compared to Fig. 3(b). But, the EIT peaks caused by $\mathbf{E}_2$ are suppressed by $\mathbf{E}_3$ because the cascade relation of G_2 and G_3 in Eq. (6). Specially, the dressing strength of $\mathbf{E}_3$ can be determined by the term of $|G_3|^2/d_3$ in Eq. (6). When $\Delta_1=0$, the value of $|G_3|^2/d_3$ becomes larger and gets maximum, so the suppression of $\mathbf{E}_3$ dressing becomes stronger which makes the peaks of EIT created by $\mathbf{E}_2$ becomes weaker. In addition, the background profile of Rydberg EIT spectrums in Fig. 4(b) shows the EIT created by $\mathbf{E}_3$ with Δ_1 scanned, which can be also explained by the term of

$|G_3|^2/d_3$ in the Eq. (5).

To further study the interaction, for simplicity, two typical values $\Delta_1=0$ and -0.1 GHz are extracted, one is doubly dressing by $|2\rangle$ and $|3\rangle$, the other one is singly dressing due to $|2\rangle$. The single dressing is not stated again because it is same with the β in Fig. 3(b). Fixing $\Delta_1=0$, Figure 4(c) shows the dependences of EIT $\rho_{10DD}^{(1)}$ (c1) and Rydberg dressing second-order fluorescence (c2) depicting by $\rho_{11DD1}^{(2)}$ on n at the same experimental condition, respectively, consisting of 37, 45, 54, and 63. The same scaling method is used to make different n possess the same Rydberg dressing effect because $I_{\text{EIT}}\propto|G_2|^2$. The spaces between the dashed line and circle dots represent the excitation blockade fraction. The variation of blockade in doubly dressing with n is obtained. It is obviously that with n increasing, EIT spectrum intensity I_{EIT} get weaker. It is clearly indicated that the Rydberg blockade strength get stronger since $G_2^{0.4}/n^{4.4}d_2$ becomes smaller when n increases. Figures 4(d1) shows the dependences of EIT spectrum intensity on G_1 and G_2, respectively. As displayed by the evolution curves and in comparison with the case of Fig. 2, the intensity varies to saturate obviously and even descends at the highest G_1 and G_2 due to adding constant dressing of $\mathbf{E}_3$. In theory, this doubly dressing effect intensity is determined in the term $G_2^{0.4}/d_2$ and $|G_3|^2/d_3$ in $\rho_{10DD}^{(1)}$. With Rabi frequency $G_1(G_2)$ increase, the variation of $G_2^{0.4}/d_2$ is the same as Fig. 2(b3). Therefore, the saturation of EIT signals is mainly caused by external dressing factor $|G_3|^2/d_3$ from $\mathbf{E}_3$.

In order to certify our conclusion, the principal quantum number n dependence of the detected Rydberg dressing second-order fluorescence dip is shown in the right panel of Fig. 4(c), which reveals the Rydberg blockade. Apparently, n increases, but the second-order fluorescence dip $\rho_{11DD1}^{(2)}$ become shallow, which results from the Rydberg blockade becomes stronger with n increasing. Figure 4(d2) shows the dependence of signals on G_1 and G_2. It indicates that the Rydberg dressing second-order fluorescence $\rho_{11DD1}^{(2)}$ almost increases linearly with Rabi frequency under the lower-excitation-Rabi-frequency condition, while the external dressing non-Rydberg second-order fluorescence $\rho_{11D2}^{(2)}$ and four-order fluorescence $\rho_{33}^{(4)}$ stay in the background. In contrary, under the higher Rabi frequency condition, the curves $\rho_{11DD1}^{(2)}$ will saturate. Such saturate trend is completely derived from suppression effect of multi-order fluorescence $\rho_{11D2}^{(2)}$ and $\rho_{33}^{(4)}$ caused by $\mathbf{E}_3$ through comparing Fig. 2(c3). In addition, the experimental results (dots) are consistent with the theoretical ones (curves).

Finally, in order to reveal Rydberg dressing more clearly, we first show the competition between Rydberg dressing second-order fluorescence $\rho_{11D1}^{(2)}$ and fourth-order fluorescence $\rho_{33}^{(4)}$ in doubly dressing as shown in Fig. (5). We still use the Y-type four level system but scan the detuning Δ_3 of $\mathbf{E}_3$,

and the $\mathbf{E}_2$ driving the Rydberg transition $|1\rangle \leftrightarrow |2\rangle$ is treated as the dressing field. With all three beams on and $P_3=32mw$, $5D_{5/2}$ state EIT spectrums versus Δ_3 when $G_1(G_2)$ increases as Fig. 5(a) shown; In every curves of Fig. 5(a), the baselines reveals the $45D_{5/2}$ Rydberg EIT induced by $\mathbf{E}_2$ at $\Delta_2+\varepsilon=-\Delta_1=0$ and the peaks over each baseline are $5D_{5/2}$ EIT induced by $\mathbf{E}_3$ at $\Delta_3=-\Delta_1$. When two EIT windows overlap at $\Delta_2+\varepsilon=\Delta_1=\Delta_3=0$, the dressing effect of $\mathbf{E}_2$ is the strongest according to $\rho_{10DD}^{(1)} \propto |G_3|^2 d_2 / |G_2|^{0.4} d_3$. With G_2 changing from 0 to $4\times2\pi$ MHz, Peaks almost does not change, which the dressing effect of $\mathbf{E}_2$ which is determined by $G_2^{0.4}/d_2$ is so weak that can not bring the influence on the EIT created by $\mathbf{E}_3$. However, $\mathbf{E}_1$ as the generation field can directly determines the EIT intensity of $\mathbf{E}_3$ and $\mathbf{E}_2$ as Fig. 5(d) shown. We can understand it by using the equation $\rho_{10DD}^{(1)} \propto G_1 /(d_1 + |G_2|^{0.4} / n^{4.4} d_2 + |G_3|^2 / d_3)$. With G_1 increasing, the EIT intensity of E_2 and E_3 become larger simultaneously. Because the EIT of $\mathbf{E}_2$ can not influence $\mathbf{E}_3$, Fig. 5(d) shows just the EIT spectrum created by $\mathbf{E}_3$. Meanwhile, the right of Fig. 5(a) and (d) agrees well with the left which shows the theoretically stimulated results.
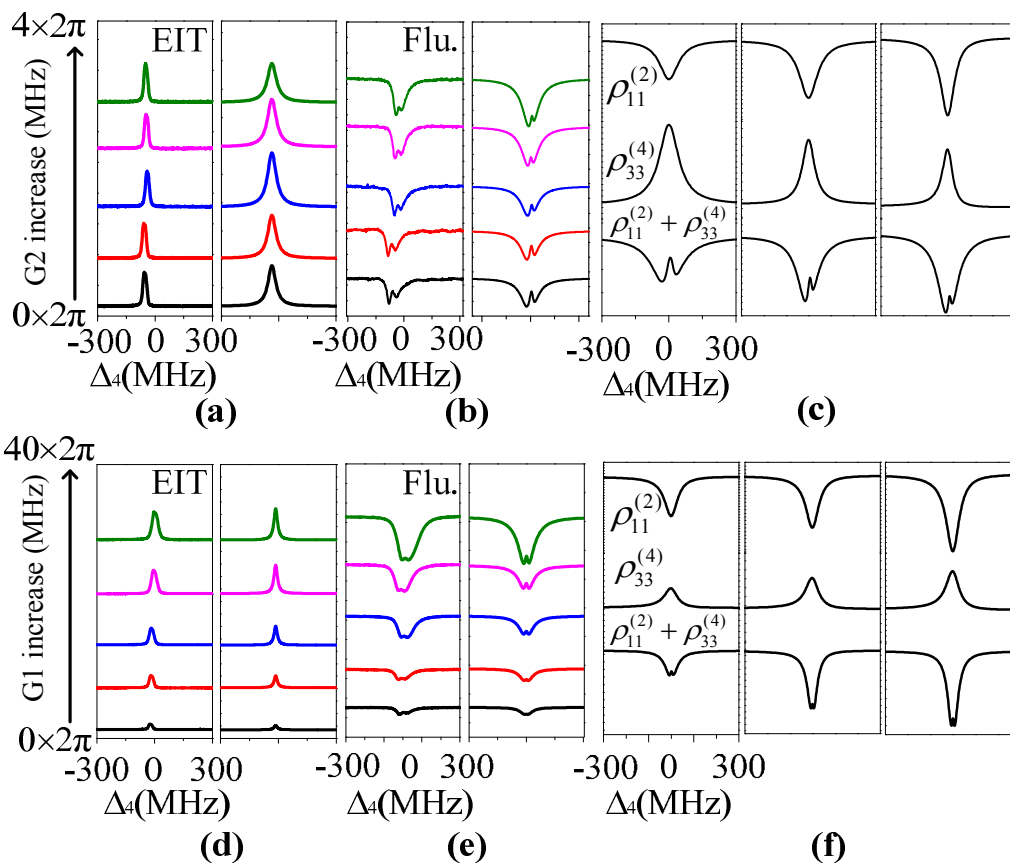

Figure 5 (color online). (a) EIT experimental signals (left) and simulations (right) under different G_2 (a1) and G_1 (a2) versus Δ_3. (b) Second-order and fourth-order fluorescence signals. Setup is as (a). (c) Simulated second-order and fourth-order fluorescence processes with G_2 (c1) and G_1 (c2). The left panel is experiment and the right simulation of (a), (b), (d) and (e).

Next, aiming at fluorescence process, Fig. 5(b) presents the fluorescence signals increasing with G_1 and G_2 from bottom to top, respectively. By scanning dressing fields, the fluorescence signals of $\mathbf{E}_3$ can be observed directly as in Fig. 5(b). In each $\mathbf{E}_3$ fluorescence signal, the doubly dressed second-order fluorescence dip generated by $\mathbf{E}_3$ is related to $\rho_{11D2}^{(2)}$. The fourth-order fluorescence (peak) within the dip R3 is determined by $\rho_{33}^{(4)}$. Rydberg dressed second-order fluorescence dip in the baseline of fluorescence signals directly interact with fluorescence of $\mathbf{E}_3$. When we change G_2 with G_1 fixed at $30\times2\pi$ MHz, The competition between the Rydberg dressed second-order fluorescence and second-order as well as fourth-order fluorescence of non-Rydberg states becomes strong. Therefore the dips $\rho_{11DD2}^{(2)}$ become deeper and the peaks $\rho_{33}^{(4)}$ become smaller, and the dips $\rho_{11DD2}^{(2)}$ rather than the peaks $\rho_{33}^{(4)}$ on fluorescence are affected by G_2 more significantly. Appearance of this result is due to two different physical mechanisms that exist in this doubly dressing fluorescence process, and one is the dressing effect of Rydberg second-order fluorescence $\rho_{11D1}^{(2)}$ plays role in the fluorescence baseline generating by coupling $5S_{1/2}$ to intermediate state $5P_{3/2}$ and interacts with non-Rydberg dressing second-order fluorescence $\rho_{11D2}^{(2)}$, the other is the Rydberg dressing second-order fluorescence $\rho_{11D1}^{(2)}$ competes with four-order fluorescence $\rho_{33}^{(4)}$. Second-order fluorescence is generated by $\rho_{00}^{(0)} \xrightarrow{E_1} \rho_{10}^{(1)} \xrightarrow{(E_1)^*} \rho_{11}^{(2)}$, fourth-order fluorescence is $\rho_{00}^{(0)} \xrightarrow{E_1} \rho_{10}^{(1)} \xrightarrow{E_3} \rho_{30}^{(2)} \xrightarrow{(E_1)^*} \rho_{31}^{(3)} \xrightarrow{(E_3)^*} \rho_{33}^{(4)}$. Rydberg dressing second-order fluorescence $\rho_{11D1}^{(2)}$ can bring the suppression on the fourth-order fluorescence $\rho_{33}^{(4)}$ and dressing intensity can be determined by the term of $G_2^{0.4}/n^{4.4}d_2$ in Eq. (14), where $d_2=\Gamma_{20}+i(\Delta_1+\Delta_2+\varepsilon)$ and $\Delta_2=0$ in experiment. With the G_2 increasing, the value of $G_2^{0.4}/n^{4.4}d_2$ becomes larger and gets maximum at $\Delta_1=0$, so the suppression of Rydberg dressing on the fourth-order fluorescence $\rho_{33}^{(4)}$ become stronger and the peaks of this fourth-order fluorescence becomes weak. More careful we find the peaks within the dips become narrow because the $\mathbf{E}_3$ fourth-order fluorescence $\rho_{33}^{(4)}$ is sheared for the second time by $\mathbf{E}_2$. For changing G_1 when $G_2=4\times2\pi$ MHz, the dips and peaks in Fig. 5(e) become larger simultaneously because the values of second-order fluorescence $\rho_{11DD2}^{(2)}$ and fourth-order fluorescence $\rho_{33}^{(4)}$ all become larger. Obviously, with G_1 increasing, the Rydberg dressed second-order fluorescence also becomes larger due to the modulation effect of $\mathbf{E}_1$ according to $\rho_{11D1}^{(2)}$, so the competition between Rydberg dressed second-order and fourth-order fluorescence become stronger In order to depict this physical process more clearly, the corresponding calculation of fluorescence signals not only represent in the right of Figs. 5(b) and (e) but also in detail show in Figs. 5(c) and (f). Especially, the calculation

$\rho_{11DD2}^{(2)}$ and $\rho_{33}^{(4)}$ are displayed separately, which can be explained as follows: The relation $\rho_{11DD2}^{(2)} \propto G_1|G_3|^2 d_2 / G_2^{0.4} d_3 d_1$ in Eq. (11) determines the depth of doubly dressing second-order fluorescence dips and $\rho_{33}^{(4)} \propto G_1^2 G_3^2 / \Gamma_{33} d_3 [d_1 + G_2^{0.4} / n^{4.4} d_2 + |G_3|^2 / d_3]$ in Eq. (14) determines the height of fourth-order fluorescence peaks, so the total intensity is $I_{\text{Flu.}} = \rho_0 \times (\rho_{11DD2}^{(2)} + \rho_{33}^{(4)})$. Such theoretical calculations confirm our experimental analysis sufficiently.

IV. CONCLUSTION

In summary, we have investigated EIT and florescence signals dressing evolution regularity with Rydberg vdW blockade based on G_1 and G_2 both theoretically and experimentally. We have certified the Rydberg vdW blockade fraction through EIT and fluorescence signals for different n in thermal environment and made use of the different degrees of dressing and blockade show the interaction between Rydberg excitation blockade and dressing effect. Meanwhile, by scanning Δ_3, the characteristic of Rydberg dressing have been investigated via interesting competition between second-order and fourth-order fluorescence. Such dressing vdW blockade signals in thermal vapor have potential application in quantum information process with Rydberg atoms as the physical carrier of qubit.

APPENDIX

symbols	Physical quantity
μ_i	Dipole moment
G_i	Rabi-frequency
ρ_e	Density of excitation Rydberg atoms
ε	Energy-level shift
n	Primarily quantum number
$\rho_{10}^{(1)}$	Density matrix of Transmission probe signals
$\rho_{11}^{(2)}$	Density matrix of second-order fluorescence signals
$\rho_{33}^{(4)}$	Density matrix of fourth-order fluorescence signals
Δ_i	Frequency detuning of E_i
Γ_{ij}	Transverse relaxation time between energy-level $|i\rangle$ and $|j\rangle$

References

1. T. F. Gallagher, *Rydberg Atoms* (Cambridge University, Cambridge, England, 1994).
2. D. Tong, S. M. Farooqi, J. Sannojevic, S. Krishnan, Y.P. Zhang, R.Côté, and M. D. Lukin, Phys. Rev. Lett. **93**, 063001(2004).
3. T. Vogt, M. Viteau, J. Zhao, A. Chotia, D. Comparat, and P. Pillet, Phys. Rev. Lett. **97**, 083003 (2006).
4. D. Jaksch, J. I. Cirac, P. Zoller, S. L. Rolston, R. Côté, and M. D. Lukin, Phys. Rev. Lett. **85**, 2208 (2000).
5. K. Tyler, G. Krittika, Y. Y. Jau, G. W. Biedermann, A. J. Landahl, and I. H. Deutsch, Phys. Rev. A. **87**, 052314 (2013).
6. M. Saffman, T. G. Walker, and K. Mölmer, Rev. Mod. Phys. **82**, 2313 (2010).
7. S. E. Harris, Phys. Today **50**, 36 (1997).
8. M. Xiao, Y. Q. Li, S. Z. Jin, and J. Gea-Banacloche, Phys. Rev. Lett. **74**, 666 (1995).
9. Y. P. Zhang, A. W. Brown, and M. Xiao, Phys. Rev. Lett, **99**, 123603 (2007).
10. Y. P. Zhang, U. Khadka, B. Anderson, and M. Xiao, Phys. Rev. Lett, **102**, 013601 (2009).
11. H. B. Zheng, X. Zhang, C. B. Li, H. Y. Lan, J. L. Che, Y. Zhang, and Y. P. Zhang, J. Chem. Phys. **138**, 204315 (2013).
12. Y. P. Zhang, Z. G. Wang, Z. Q. Nie, C. B. Li, H. X. Chen, K. Q. Lu, and M. Xiao, Phys. Rev. Lett, **106**, 093904 (2011).
13. A. K. Mohapatra, T. R. Jackson, and C. S. Adams, Phys. Rev. Lett. **98**, 113003 (2007).
14. B. Huber, T. Baluktsian, M. Schlagmüller, A. Kölle, H. Kübler, R. Löw, and T. Pfau, Phys. Rev. Lett. **107**, 243001 (2011).
15. T. Baluktsian, B. Huber, R. Löw, and T. Pfau, Phys. Rev. Lett. **110**, 123001 (2013).
16. K. Singer, J. Stanojevic, M. Weidemüller, and R. Côté, J. Phys. At. Mol. Opt. Phys. **38**, S295 (2005).
17. J. Sun, Z. C. Zuo, X. Mi, Z. H. Yu, Q. Jiang, Y. B. Wang, L. A. Wu, and P. M. Fu, Phys. Rev. A. **70**, 053820(2004).
18. Z. Q. Nie, H. B. Zheng, P. Z. Li, Y. M. Yang, Y. P. Zhang, and M. Xiao, Phys. Rev. A. **77**, 063829 (2008).
19. S. Sevincli, N. Henkel, C. Ates, and T. Pohl, Phys. Rev. Lett. **107**, 153001, (2011).